



ISTITUTO NAZIONALE DI RICERCA METROLOGICA Repository Istituzionale

Symmetric autobalanced Ramsey interrogation for high-performance coherent-population-trapping vapor-cell atomic clock

Original

Symmetric autobalanced Ramsey interrogation for high-performance coherent-population-trapping vapor-cell atomic clock / Abdel Hafiz, M.; Coget, G.; Petersen, M.; Calosso, C. E.; Guérandel, S.; de Clercq, E.; Boudot, R.. - In: APPLIED PHYSICS LETTERS. - ISSN 0003-6951. - 112:24(2018), p. 244102. [10.1063/1.5030009]

Availability:

This version is available at: 11696/59843 since: 2021-03-08T20:18:07Z

Publisher:

APPLIED PHYSICS LETTERS

Published

DOI:10.1063/1.5030009

Terms of use:

This article is made available under terms and conditions as specified in the corresponding bibliographic description in the repository

Publisher copyright

(Article begins on next page)

Symmetric autobalanced Ramsey interrogation for high-performance coherent-population-trapping vapor-cell atomic clock

Cite as: Appl. Phys. Lett. **112**, 244102 (2018); <https://doi.org/10.1063/1.5030009>

Submitted: 18 March 2018 . Accepted: 30 May 2018 . Published Online: 13 June 2018

M. Abdel Hafiz, G. Coget, M. Petersen,  C. E. Calosso, S. Guérandel, E. de Clercq, and  R. Boudot



View Online



Export Citation



CrossMark

ARTICLES YOU MAY BE INTERESTED IN

[A high-performance Raman-Ramsey Cs vapor cell atomic clock](#)

Journal of Applied Physics **121**, 104903 (2017); <https://doi.org/10.1063/1.4977955>

[Chip-scale atomic devices](#)

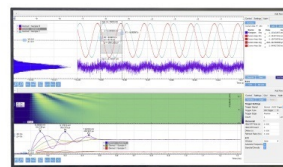
Applied Physics Reviews **5**, 031302 (2018); <https://doi.org/10.1063/1.5026238>

[Power stabilization of a diode laser with an acousto-optic modulator](#)

Review of Scientific Instruments **89**, 113112 (2018); <https://doi.org/10.1063/1.5046852>

Challenge us.

What are your needs for
periodic signal detection?



Zurich
Instruments



Symmetric autobalanced Ramsey interrogation for high-performance coherent-population-trapping vapor-cell atomic clock

M. Abdel Hafiz,¹ G. Coget,¹ M. Petersen,¹ C. E. Calosso,² S. Guérandel,³ E. de Clercq,³ and R. Boudot^{1,a)}

¹FEMTO-ST, CNRS, UBFC, 26 rue de l'épître 25030 Besançon, France

²INRIM, Strada delle Cacce 91, 10135 Torino, Italy

³LNE-SYRTE, Observatoire de Paris, Université PSL, CNRS, Sorbonne Université, 61 avenue de l'Observatoire, 75014 Paris, France

(Received 18 March 2018; accepted 30 May 2018; published online 13 June 2018)

We report a high-performance pulsed coherent population trapping (CPT) Cs cell atomic clock using the implementation of a symmetric auto-balanced Ramsey (SABR) interrogation sequence. The latter method is found to reduce the light-power induced frequency shift by an order of magnitude compared to a previous experiment using a simple auto-balanced Ramsey interrogation. The contribution of this shift to the clock frequency stability is now rejected in the 10^{-16} range at 10^4 s averaging time. Additional tricks, including a compensation method to reduce the laser amplitude noise contribution and the generation of novel error signals for local oscillator frequency and phase correction, have been implemented using a FPGA-based digital electronics board in order to improve the clock short-term stability by a factor of 2. The Allan deviation of the SABR-CPT clock, extracted from a selected 3×10^4 s-long dataset, is $2 \times 10^{-13} \tau^{-1/2}$ and averages down to the level of 2.5×10^{-15} at 10^4 s. These results are encouraging to stimulate the development of hot cell CPT-based clocks for industrial, scientific, and instrumentation applications. *Published by AIP Publishing.* <https://doi.org/10.1063/1.5030009>

Compact vapor cell atomic clocks are high-precision time and frequency instruments that exhibit a strong potential for deployment and commercialization in a wide variety of applications including telecommunication network synchronization, secure data transfer, satellite-based inertial navigation, defense, geodesy, or smart power grids. Widely used devices are commercial Cs beam clocks¹ and double-resonance Rb vapor cell clocks,^{2,3} both offering for time scales higher than 10^2 – 10^3 s frequency stability performances which are superior to quartz oscillators while maintaining a modest volume, power consumption, and cost. Different approaches have been proposed for the development of new-generation high-performing vapor-cell compact atomic clocks.⁴ The pulsed optically pumped (POP) Rb frequency standard has demonstrated outstanding performances with a fractional frequency stability of $1.7 \times 10^{-13} \tau^{-1/2}$ up to 1000 s and at the level of 10^{-14} at 10^5 s.⁵ Similar short-term stabilities have been obtained with revisited double-resonance schemes, pumped by lamps⁶ or by lasers.⁷

An alternative approach is the development of atomic clocks based on coherent population trapping (CPT).^{8,9} This method, well-recognized for having permitted the commercialization of chip-scale atomic clocks,^{10–12} has already demonstrated competitive short-term instabilities at the level of 2 – $4 \times 10^{-13} \tau^{-1/2}$.^{13–16} However, these clocks suffer in general on time scales longer than 100 s from significant frequency instabilities mainly attributed to light-induced frequency shift effects.

An elegant approach to reduce this major contribution is to probe the atoms with a pulsed Ramsey-CPT sequence.¹⁷

This method allows the detection of narrow Ramsey-CPT fringes whose linewidth is mainly dependent on the free-evolution time and poorly affected by the power broadening and for which resonant light shifts scale inversely with the free-evolution time in the dark.^{15,18,19} However, the Ramsey-CPT interrogation exhibits a non-negligible residual sensitivity to light-shift effects.

In a recent work, we have proposed the application of the auto-balanced Ramsey (ABR) interrogation protocol^{20,21} onto a pulsed CPT-based Cs cell clock.²² This method is based on the alternation of two successive Ramsey-CPT sequences with unequal free-evolution times and the subsequent management of two interleaved phase and frequency servo loops. This approach has demonstrated a reduction of the CPT clock frequency sensitivity to laser power variations, yielding a clock Allan deviation of $3.1 \times 10^{-13} \tau^{-1/2}$ averaging down to 6×10^{-15} at 2000 s. In this study, it was also reported that the clock short-term frequency stability in the ABR-CPT regime was slightly degraded by a factor 2 compared to the Ramsey-CPT regime, due to the modified clock cycle time and sequence.

In the present paper, we report that an atomic memory effect, explained by the fact that the repetition rate of the successive Ramsey sequences is faster than the CPT coherence relaxation rate, induces in the ABR-CPT regime a frequency-error in the light-shift estimation. The atomic signal level detected at a given CPT pulse depends also on the previous CPT pulses. If not suppressed, this effect prevents a complete cancellation of the probing-field induced frequency shift and limits the efficiency of the ABR-CPT protocol.

To tackle this issue, we demonstrate here the implementation of a symmetric ABR-CPT (SABR-CPT) interrogation

^{a)}Electronic mail: rodolphe.boudot@femto-st.fr

sequence that allows the generation of two successive offsets with equal modulus and opposite sign that cancel each other. While representing a minor modification to apply in the sequence from an experimental point of view, the SABR-CPT protocol is found to reduce by a supplemental order of magnitude the dependence of the clock frequency to laser-power variations. Additionally, we report the real-time processing of novel error signals and the implementation of a simple compensation method that reduces the laser amplitude (AM) noise contribution. This yields a gain of a factor 2 on the clock short-term stability. These efforts conduct to the demonstration over a selected 3×10^4 s-dataset measurement of a hot vapor Cs cell clock with an Allan deviation of $2 \times 10^{-13} \tau^{-1/2}$, averaging down to the level of 2×10^{-15} at 10^4 s.

Figure 1 describes the Cs CPT clock experimental setup. The optical part has already been described in detail in Ref. 15. Only main points are here recalled. The light of a distributed feedback (DFB) diode laser is injected into a fibered Mach-Zehnder electro-optic modulator (EOM) driven at 4.596 GHz in order to produce two first-order optical sidebands frequency-split by 9.192 GHz for CPT interaction. The laser first-order sideband frequencies are connected and stabilized to the Cs D₁ line at 894.6 nm using a dual-frequency Doppler-free spectroscopy setup.^{23,24} An acousto-optical modulator (AOM) shifts the laser frequencies by -122 MHz to compensate for the buffer-gas induced optical frequency shift²⁵ in the CPT cell, controls the laser power, and produces the optical CPT pulse sequence. A Michelson-like system produces the two bi-chromatic optical fields with orthogonal circular polarizations and a half-clock period delay of the push-pull optical pumping scheme^{26,27} (PPOP). Before the CPT cell, a fraction of the light is now reflected by a cube and recorded by the photodiode PD2. The transmitted light crosses a 5-cm long and 2-cm diameter Cs vapor cell filled with 15 Torr of a N₂-Ar buffer gas mixture (pressure ratio $P_{Ar}/P_{N_2} = 0.6$).²⁸ A longitudinal static magnetic field of 50 mG is applied. A double-layer mu-metal magnetic shield surrounds the cell package. The light transmitted through the cell is detected by the photodiode PD1.

The local oscillator (LO) is an ultra-low phase noise 100 MHz oven-controlled quartz crystal oscillator (OCXO). This source is frequency multiplied to 4.596 GHz with a low noise microwave frequency synthesis chain.²⁹ The clock operation (except for the laser head) is piloted now by a

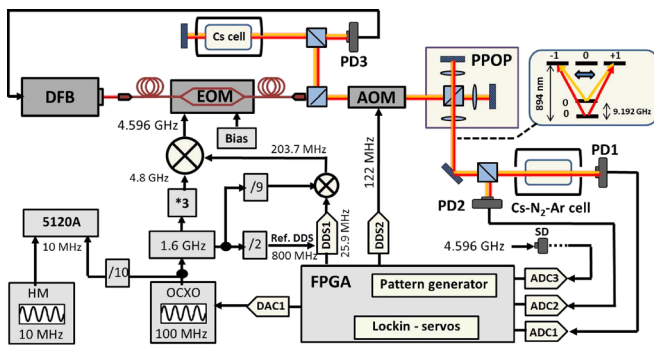


FIG. 1. ABR-CPT clock setup. The bias box is a bias voltage applied to allow the optical carrier suppression at the output of the EOM. All acronyms are defined in the text. The inset shows the CPT scheme diagram involved in the experiment.

single digital electronics board.³⁰ The latter integrates a direct digital synthesis (DDS1: 25.9 MHz output) for the microwave synthesis chain, a second DDS (DDS2: 122 MHz output) to drive the AOM and apply the light pulse sequence, three 18-bit analog-to-digital converters (ADCs) to acquire the atomic signal (PD1 signal), the photodiode PD2 signal, and the 4.596 GHz signal microwave power (through the use of a Schottky diode), and a digital-to-analog converter (DAC) to drive the OCXO frequency. All these elements are interfaced with a central FPGA that pilots the clock. The OCXO output signal is frequency-divided from 100 MHz to 10 MHz and is compared to the 10 MHz signal from an active hydrogen maser using a phase noise and Allan deviation test set (Microsemi 5120A).

Figure 2 describes the SABR-CPT sequence. Optical CPT pulses of length 1.1 ms are used for both CPT pumping and CPT detection and are separated by unequal free-evolution dark times. On each pulse, a time delay τ_d of 20 μ s is applied before opening a detection window τ_D of length 120 μ s during which the atomic signal (PD1) and the laser power signal (PD2) are averaged.

The sequence is divided into two basic sub-sequences (white and pink areas in Fig. 2), each of them consisting of two short dark times (T_S) followed by two long dark times (T_L). In the first sub-sequence, similar to the one applied in Ref. 22, the signal is successively measured on the left (l) and on the right (r) of the central Ramsey-CPT fringe for both T_S and T_L dark time windows, producing two successive error signals ε_S (for T_S) and ε_L (for T_L). A $\pi/2$ phase modulation is applied onto the Raman phase using DDS1 during the dark time for this purpose. An additional phase jump φ_c , generated to compensate for the probing-field induced clock frequency shift,²⁰ is applied just after each $\pm\pi/2$ jump. In our experiment, due to the lack of phase resolution of the DDS1, this phase jump is applied by producing a frequency jump $\Delta\nu_c$ during a time window Δt . In Ref. 22, the error signal ε_S extracted from the cycle with $T_R = T_S$ was used to compute the value of the phase jump φ_c applied in the next iteration, while the error signal ε_L extracted from the cycle with $T_R = T_L$ was used to correct the LO frequency. At the end, the control electronics manages two interleaved phase and frequency servo loops targeting to null both signals ε_S

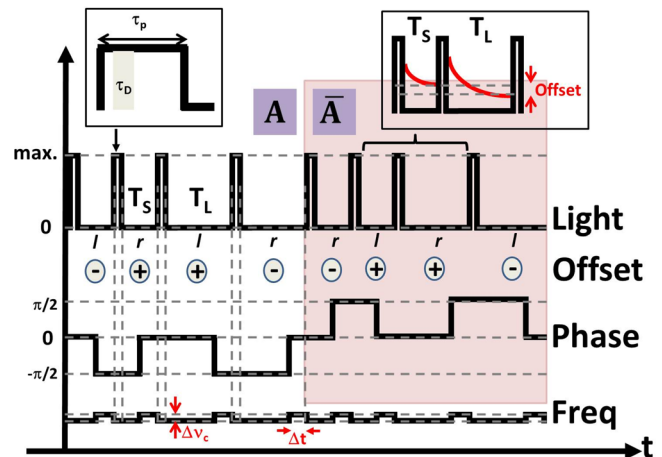


FIG. 2. SABR-CPT sequence.

and ε_L . A correction is applied to the LO frequency and to the phase-jump value φ_c at the end of each sequence, just after the last detection window.

While demonstrating encouraging performances, we have observed in the ABR-CPT configuration described in Ref. 22 that the sensitivity of the clock frequency to laser power variations could be minimized by adding a slight voltage offset to the error signal of the phase loop, indicating that a fraction of the light shift was not correctly detected and/or compensated. We now explain this behavior by an atomic memory effect. Since the light pulses are too short to get the steady-state and since the coherence lifetime T_2 (~ 3 ms) is not short compared to the length of a Ramsey sequence (~ 3 – 6 ms), the signal level detected at a given CPT pulse depends on the length of the two previous dark times. Consequently, the fringe signal detected at the end of a short (or long) free-evolution time is slightly increased when the preceding dark time is short. In contrast, the fringe signal is slightly decreased if the preceding dark time is long. Depending on whether the preceding dark time is short or long, these voltage offsets induce in the light-shift estimation slight frequency offsets of opposite sign, noted in Fig. 2 \oplus and \ominus , respectively. We note that the application of the ABR protocol on this CPT experiment is in that sense notably different from the situation encountered in the Yb^+ ion clock experiment on which the ABR method was first proposed and where successive Ramsey sequences are fully independent.²⁰

To tackle the above-mentioned issue, we have implemented as shown in Fig. 2 the SABR-CPT interrogation sequence. In the second sub-sequence (pink area of Fig. 2), the phase of the interrogating signal is now changed with opposite sign, meaning that the signal readout is performed first on the right (r) part of the fringe and then on the left (l) part. The SABR-CPT protocol sequence allows the generation of two successive offsets (noted A and \bar{A} in Fig. 2) with

equal modulus and opposite sign that cancel each other, yielding to enhance the rejection of light-shift effects.

Efforts were also pursued to improve the clock short-term stability in the ABR-CPT regime. In Ref. 22, the latter was found to be slightly degraded by a factor 2 in the ABR-CPT method compared to the usual Ramsey-CPT case. This degradation was partly explained by the fact that cycles dedicated to the LO phase correction act as a dead time (loss of information) for the LO frequency servo loop.²⁹ To respond to this issue, we have implemented the real-time calculation of two novel error signals. The sum $\varepsilon_+ = \varepsilon_S + \varepsilon_L$ of the two error signals is used to correct the LO frequency, while the difference $\varepsilon_- = \varepsilon_S - \varepsilon_L$ is extracted to correct the phase-jump value φ_c . In that way, all pulses are exploited to extract some useful information for correction of both the phase-jump value and frequency.

In Ref. 22, the clock short-term stability in the ABR-CPT regime was mainly limited by the laser AM noise. In order to reduce this contribution, the system now acquires the voltage signals V_1 and V_2 from photodiodes PD1 and PD2, respectively. The useful signal managed in clock operation to extract error signals is then $V = V_1 - kV_2$, where k is a compensation factor to be adjusted. Similar techniques have been used in the literature.³¹ This method was found to improve the clock short-term frequency stability in the ABR-CPT regime by a factor 2.

Figure 3 shows typical error signals managed in the ABR-CPT clock experiment. This includes the error signal ε_L extracted from a long dark time ($T_L = 4$ ms) (a), the error signal ε_S extracted from a short dark time ($T_S = 1$ ms) (b), the sum of both error signals $\varepsilon_+ = \varepsilon_L + \varepsilon_S$ (c), and the difference of both error signals $\varepsilon_- = \varepsilon_S - \varepsilon_L$ (d).

Figure 4 reports the frequency shift (referred to 9.192639290 GHz, i.e., the clock frequency buffer-gas shifted by +7520 Hz from the unperturbed Cs atom frequency) versus the laser power P_L , the laser frequency f_L , the

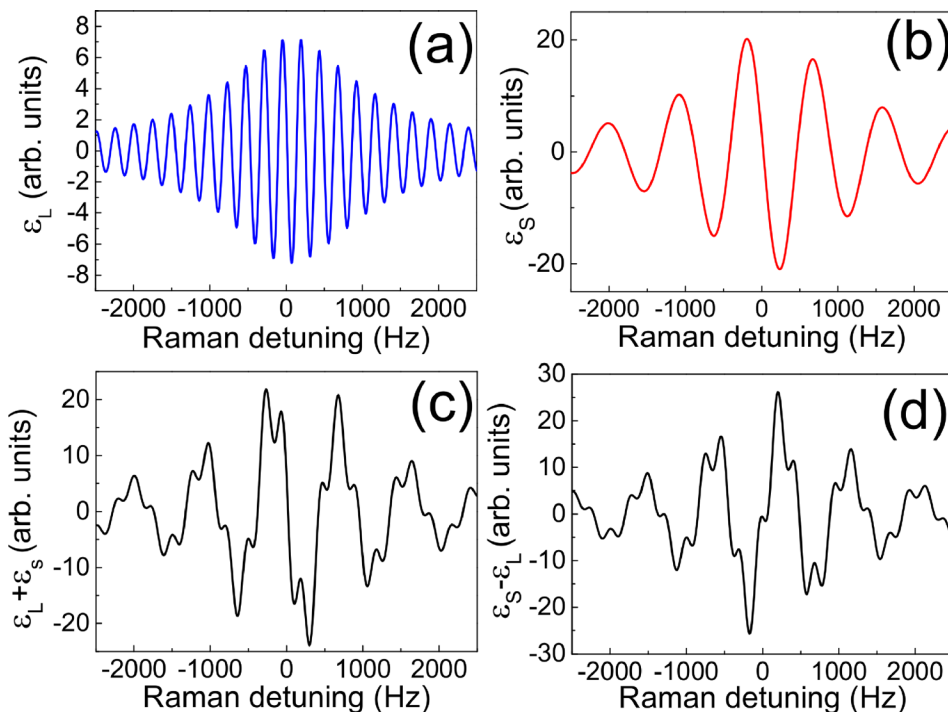


FIG. 3. Error signals managed in the ABR-CPT clock. (a) ε_L ($T_L = 4$ ms), (b) ε_S ($T_S = 1$ ms), (c) $\varepsilon_+ = \varepsilon_L + \varepsilon_S$, and (d) $\varepsilon_- = \varepsilon_S - \varepsilon_L$. Values used here are $\tau_p = 1.1$ ms, $\tau_D = 120$ μ s, and $\tau_d = 20$ μ s.

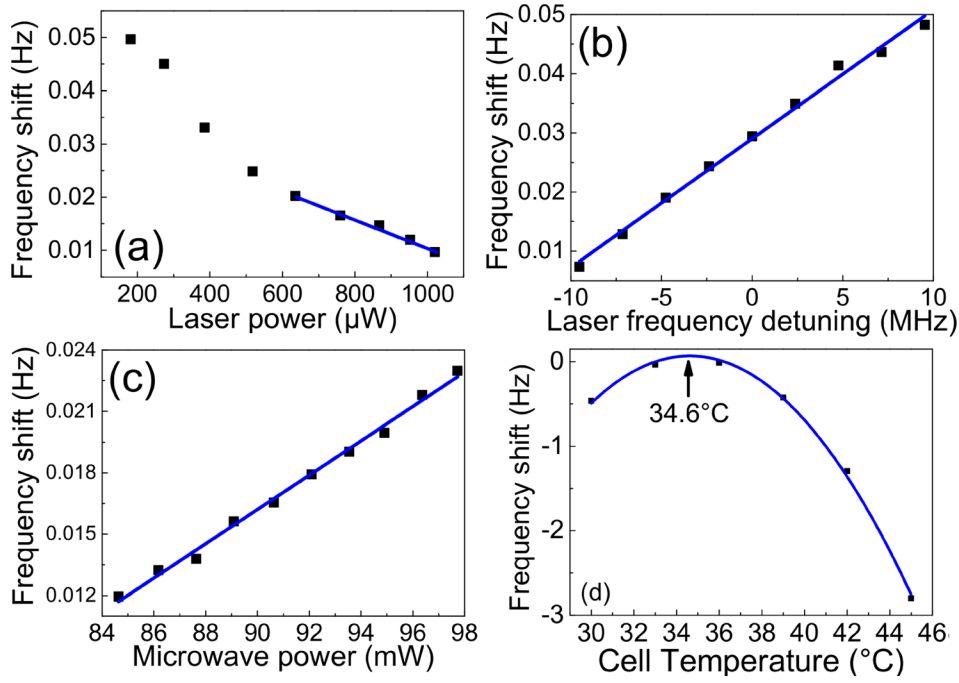


FIG. 4. Frequency shift (from 9.192639290 GHz, the clock frequency) versus the laser power (a), the laser frequency (b), the microwave power at 4.6 GHz injected into the EOM (c), and the cell temperature (d). For (d), data points are measured at a laser power of 800 μ W.

microwave power P_μ , and the cell temperature T_{cell} , respectively. The clock frequency-laser power dependence is found to be non-linear in the 150–1000 μ W range. However, around the typical laser power working point used in the clock configuration ($\sim 850 \mu$ W), the sensitivity of the clock frequency to laser power variations can be reasonably fitted by a linear function and is reduced to only $-2.9 \times 10^{-15}/\mu$ W, in fractional value. This coefficient is about 10 times lower than with our first ABR-CPT test,²² 80 times lower than in the Ramsey-CPT case¹⁵ and about 800 times smaller than in the continuous CPT regime.¹⁴ This gain is the direct consequence of the SABR-CPT interrogation sequence.

The dependence of the clock frequency to the laser frequency is well-approximated by a linear function in the studied range, yielding a residual sensitivity in the fractional value of $2.4 \times 10^{-13}/\text{MHz}$. This value is comparable to the one measured in the conventional Ramsey-CPT regime.^{14,15} The sensitivity of the clock frequency to microwave power variations is measured to be in the fractional value of about $10^{-13}/\%$. This coefficient is about 5 times lower than the one obtained in the Ramsey-CPT case. The explanation of these residual sensitivities remains to be determined. In our experiment, the temperature dependence of the clock frequency is canceled at the first-order around an inversion temperature of about 34.6 $^{\circ}\text{C}$ [Fig. 4(d)].²⁸ Fitting experimental data by a second-order polynomial function, the residual cell temperature dependence of the fractional clock frequency shift around this point is estimated to be $8 \times 10^{-11} \text{ K}^{-2}$.

Figure 5 reports the Allan deviation of the clock frequency obtained in different conditions and distinct moments. Measurements (a) and (b) were previously reported in Ref. 22 and are shown for comparison. In both cases (a) and (b), a high-bandwidth laser power servo loop was used. The latter allowed in reducing the detection noise at the clock cycle frequency (then optimizing the clock short-term stability) but also laser power fluctuations at 10^4 s by a factor 40 compared to the free-running regime.²² In curve (a), the clock was operated in the usual Ramsey-CPT

regime ($T_R = 2.7$ ms). In this case, the clock frequency stability was optimized at the level of $1.45 \times 10^{-13} \tau^{-1/2}$ up to 200 s, degrading after to reach the level of 10^{-13} at 10^4 s. In case (b), the clock was operated in the ABR-CPT regime²² with a single ABR-CPT sub-sequence. The clock Allan deviation, extracted from a selected limited duration dataset where environmental conditions were quiet, was measured to be $3.1 \times 10^{-13} \tau^{-1/2}$, averaging down to 6×10^{-15} at 2000 s.

Measurements (c) and (d) are the results from the present study with the SABR-CPT protocol. Here, only a low-bandwidth laser power servo loop is active. The latter does not help to improve the short-term stability but allows to reach a similar level of relative power fluctuations at 10^4 s than the previous power servo system. The laser AM noise compensation method described above is turned off for (c) and active for (d). Data of curve (c) are extracted from a 5-day measurement. Here, the clock short-term frequency stability in the ABR-CPT regime is slightly degraded compared

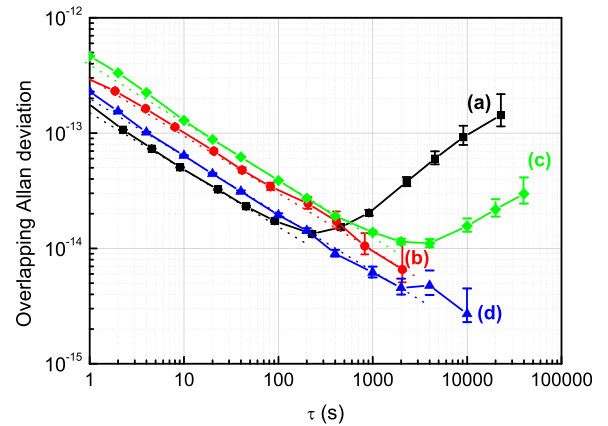


FIG. 5. Allan deviation of the clock frequency. (a): Ramsey-CPT regime ($T_R = 2.7$ ms),²² (b) ABR-CPT regime with a single sub-sequence,²² (c) SABR-CPT regime with two sub-sequences, 5-days measurement, normalization method off, and (d) SABR-CPT regime with two sub-sequences, selected 30 000 s-dataset, normalization method active. Dotted lines are $\tau^{-1/2}$ -slope fit curves to the data.

TABLE I. Typical clock stability budget at $\tau = 10^4$ s.

| Source | Sensitivity | Fluctuations | $\sigma_y(\tau)$ (10^{-15}) |
|-------------------|-----------------------------------|------------------------------|---------------------------------|
| P_L | $2.9 \times 10^{-15}/\mu\text{W}$ | $0.085 \mu\text{W}$ | 0.25 |
| f_L | $2.4 \times 10^{-13}/\text{MHz}$ | 3.35 kHz | 0.8 |
| B | $4.6 \times 10^{-9}/\text{G}$ | $4 \times 10^{-7} \text{ G}$ | 1.85 |
| P_μ | $1 \times 10^{-13}/\%$ | $<0.01\%$ | <1 |
| T_{cell} | $8 \times 10^{-11}/\text{K}^{-2}$ | $<10^{-4} \text{ K}$ | <0.8 |

to curve (b) to $4 \times 10^{-13} \tau^{-1/2}$ due to the limited bandwidth of the laser power servo loop. For averaging times higher than 3000 s, the clock Allan deviation evolves with $1.5 \times 10^{-16} \sqrt{\tau}$, signature of a frequency random walk, and is 3×10^{-14} at 4×10^4 s. The Allan deviation plot of curve (d) is extracted from a selected 30 000-s duration dataset with quiet environmental conditions. In this case, the clock short-term stability is improved by a factor 2 compared to (c) thanks to the normalization method. Note that the latter only helps to reduce the detection noise at the clock cycle frequency and then the short-term stability but does not explain in curve (d) the stability improvement after 1000 s in comparison with (c). This measurement also shows that the clock stability may reach the level of 2.5×10^{-15} at 10^4 s.

Table I resumes some usual main contributions to the clock stability at 10^4 s in the SABR-CPT regime, with active laser power servo.

The outstanding result from this analysis is that the SABR-CPT protocol allows us to reject the contribution of the laser-power induced shift at the negligible level of 2.5×10^{-16} at 10^4 s. This led the clock to reproducibly reach the level of 2.5×10^{-15} for short measurement times. Other contributions studied here are found to be roughly of equal importance (close to the 10^{-15} level) and will have to be considered with precaution.

For long-duration measurements (curve c), investigations are still in-progress to identify the main source of degradation of the clock frequency stability. This supplemental frequency instability is suspected to be linked to temperature variations or atmospheric pressure variations of the experimental setup. A relevant correlation between the clock frequency and both the AOM and laser head system temperatures has been observed. Other possible causes, unexplored to date in the ABR-CPT regime, could be frequency shifts induced by variations of the light field polarization, sideband asymmetry,^{32,33} or phase chirps and Zeeman shifts.²⁰ All these aspects will be studied in detail in a near future.

This work was supported by LNE and LabeX FIRST-TF. The authors thank C. Rocher and P. Abbé (FEMTO-ST) for their help with experimental stuff.

¹L. S. Cutler, *Metrologia* **42**, S90 (2005).

²J. Vanier and C. Mandache, *Appl. Phys. B* **87**, 565 (2007).

- ³V. Formichella, J. Camparo, and P. Tavella, *Appl. Phys. Lett.* **110**, 043506 (2017).
- ⁴A. Godone, F. Levi, C. E. Calosso, S. Micalizio, and A. Godone, *Riv. Nuovo Cimento* **38**, 133–171 (2015).
- ⁵S. Micalizio, C. E. Calosso, A. Godone, and F. Levi, *Metrologia* **49**, 425–436 (2012).
- ⁶Q. Hao, W. Li, S. He, J. Lv, P. Wang, and G. Mei, *Rev. Sci. Instrum.* **87**, 123111 (2016).
- ⁷M. Gharavipour, C. Affolderbach, S. Kang, T. Bandi, F. Gruet, M. Pellaton, and G. Milet, *J. Phys.: Conf. Ser.* **723**, 012006 (2016).
- ⁸G. Alzetta, A. Gozzini, L. Moi, and G. Orriols, *Nuovo Cimento B* **36**, 5 (1976).
- ⁹J. Vanier, *Appl. Phys. B: Lasers Opt.* **81**, 421 (2005).
- ¹⁰S. Knappe, V. Shah, P. D. D. Schwindt, L. Hollberg, J. Kitching, L. A. Liew, and J. Moreland, *Appl. Phys. Lett.* **85**(9), 1460–1462 (2004).
- ¹¹S. Knappe, “MEMS atomic clocks,” in *Comprehensive Microsystems*, edited by Y. Gianchandani, O. Taba, and H. Zappe (Elsevier B. V., Maryland Heights, MO, 2007), Vol. 3, pp. 571–612.
- ¹²R. Lutwak, A. Rashed, M. Varghese, G. Tepolt, J. Leblanc, M. Mescher, D. K. Serkland, and G. M. Peake, in *Proceedings of 2007 International Frequency Control Symposium and European Frequency and Time Forum (EFTF) Joint Meeting*, Geneva, France, pp. 1327–1333.
- ¹³J. M. Danet, M. Lours, S. Guérandel, and E. De Clercq, *IEEE Trans. Ultrason. Ferroelectr. Freq. Control* **61**(4), 567 (2014).
- ¹⁴M. Abdel Hafiz and R. Boudot, *J. Appl. Phys.* **118**, 124903 (2015).
- ¹⁵M. Abdel Hafiz, G. Coget, P. Yun, S. Guérandel, E. de Clercq, and R. Boudot, *J. Appl. Phys.* **121**, 104903 (2017).
- ¹⁶P. Yun, F. Tricot, C. E. Calosso, S. Micalizio, B. Francois, R. Boudot, S. Guérandel, and E. de Clercq, *Phys. Rev. Appl.* **7**, 014018 (2017).
- ¹⁷T. Zanon, S. Guérandel, E. de Clercq, D. Holleville, N. Dimarcq, and A. Clairon, *Phys. Rev. Lett.* **94**, 193002 (2005).
- ¹⁸E. Blanshan, S. M. Rochester, E. Donley, and J. Kitching, *Phys. Rev. A* **91**, 041401(R) (2015).
- ¹⁹X. Liu, E. Ivanov, V. I. Yudin, J. Kitching, and E. A. Donley, *Phys. Rev. Appl.* **8**, 054001 (2017).
- ²⁰C. Sanner, N. Huntemann, R. Lange, C. Tann, and E. Peik, *Phys. Rev. Lett.* **120**, 053602 (2018).
- ²¹V. Yudin, A. V. Taichenachev, M. Y. Basalaev, T. Zanon-Willette, J. W. Pollock, M. Shuker, E. A. Donley, and J. Kitching, *Phys. Rev. Appl.* **9**, 054034 (2018).
- ²²M. Abdel Hafiz, G. Coget, M. Petersen, C. Rocher, T. Zanon-Willette, S. Guérandel, E. de Clercq, and R. Boudot, *Phys. Rev. Appl.* **9**, 064002 (2018).
- ²³M. Abdel Hafiz, G. Coget, E. De Clercq, and R. Boudot, *Opt. Lett.* **41**(13), 2982 (2016).
- ²⁴M. Abdel Hafiz, D. Brazhnikov, G. Coget, A. Taichenachev, V. Yudin, E. de Clercq, and R. Boudot, *New J. Phys.* **19**, 073028 (2017).
- ²⁵G. A. Pitz, D. E. Wertepny, and G. P. Perram, *Phys. Rev. A* **80**, 062718 (2009).
- ²⁶Y. Y. Jau, E. Miron, A. B. Post, N. N. Kuzma, and W. Happer, *Phys. Rev. Lett.* **93**, 160802 (2004).
- ²⁷X. Liu, J. M. Mérolla, S. Guérandel, C. Gorecki, E. de Clercq, and R. Boudot, *Phys. Rev. A* **87**, 013416 (2013).
- ²⁸O. Kozlova, E. de Clercq, and S. Guérandel, *Phys. Rev. A* **83**, 062714 (2011).
- ²⁹B. François, C. E. Calosso, M. Abdel Hafiz, S. Micalizio, and R. Boudot, *Rev. Sci. Instrum.* **86**, 094707 (2015).
- ³⁰C. E. Calosso *et al.*, in *Local Oscillators and Digital Electronics for Compact Atomic Clocks, Microwave Technology and Techniques Workshop*, ESA-ESTEC, Noordwijk, 3–5 April 2017 (2017).
- ³¹V. Gerginov, S. Knappe, V. Shah, L. Hollberg, and J. Kitching, *IEEE Trans. Instrum. Meas.* **57**(7), 1357–1361 (2008).
- ³²O. Kozlova, J. M. Danet, S. Guérandel, and E. de Clercq, *IEEE Trans. Instrum. Meas.* **63**, 1863–1870 (2014).
- ³³J. W. Pollock, V. I. Yudin, M. Shuker, M. Y. Basalaev, A. V. Taichenachev, X. Liu, J. Kitching, and E. A. Donley, preprint [arXiv:1805.06029](https://arxiv.org/abs/1805.06029) (2018).